

# LHC INTERACTION REGION QUADRUPOLE ERROR IMPACT STUDIES\*

W. Fischer, V. Ptitsin and J. Wei, BNL, USA; R. Ostojic, CERN, Switzerland; J. Strait, FNAL, USA

## Abstract

The performance of the Large Hadron Collider (LHC) at collision energy is limited by the field quality of the interaction region (IR) quadrupoles and dipoles. In this paper we study the impact of the expected field errors of these magnets on the dynamic aperture. We investigate different magnet arrangements and error strength. Based on the results we will propose and evaluate a corrector layout to meet the required dynamic aperture performance in a companion paper.

## 1 INTRODUCTION

The LHC interaction region consists of a low- $\beta$  quadrupole triplet (Q1-Q3) and a separation dipole (D1) on either side of the interaction point (IP), as shown in Fig. 1. The superconducting triplet quadrupoles are built by FNAL and KEK, and assembled in cryostats at FNAL. The separation dipoles in the high luminosity interactions points IP1 (ATLAS) and IP5 (CMS) are room-temperature magnets supplied by IPN-Novosibirsk. In IP2 (ALICE) and IP8 (LHC-B), where the beams are injected into the two rings, the D1 magnets are superconducting, built by BNL.

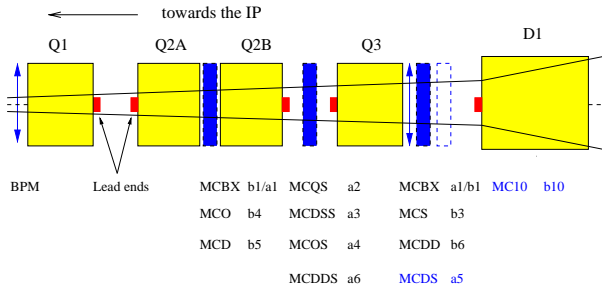


Figure 1: Schematic layout of the LHC inner triplet region.

The target dynamic aperture for the magnet field quality is set at 12 times the transverse rms beam size ( $12\sigma_{xy}$ ) after 100,000 turns, for both injection and collision. During injection and ramping, the impact of IR magnets is small compared with that of the arc magnets. On the other hand, during p-p collisions the reduction of beam size at IP1 and IP5 results in a large beam size ( $\sigma_{xy} = 1.5\text{mm}$ ) at the corresponding triplets (Tab. 1). Furthermore, beam-beam interactions require a crossing angle of  $\pm 150\mu\text{r}$  corresponding to a closed orbit of up to  $\pm 7.3\text{mm}$ . The target  $12\sigma_{xy}$

Table 1: LHC parameters for protons at collision (7 TeV).

|  |                                |
|--|--------------------------------|
| tunes H/V/L                                | 63.31/59.32/0.00212            |
| $\beta^*$ IP1,5,2,8 H/V [m]                | 0.5/0.5, 0.5/0.5, 15/10, 13/15 |
| $\Phi/2$ IP1,5,2,8 H/V [ $\mu\text{rad}$ ] | 0/150, 150/0, 0/-150, 0/-150   |
| max rms beam size [mm]                     | 1.5                            |
| max orbit offset H/V [mm]                  | $\pm 7.3/\pm 7.3$              |

thus corresponds to about 71% of the magnet coil radius. Similarly, during ion collision [1] when the beam size is squeezed at IP2, the impact from the cold D1 is also noticeable. Compensation of field errors of the cold IR magnets is of primary importance in improving the performance of the LHC at collision [2].

The impact of IR magnetic field errors has been analysed previously [3, 4]. Since the first field quality analysis of the US-LHC magnets [3], there have been several iterations of design and test of the magnets that lead to improvements of the field quality. For the FNAL-built quadrupoles, the systematic  $b_6$  in the lead end and the systematic  $b_{10}$  in the body have both been reduced; the random  $b_3$  and  $b_4$  in the body are small compared with the first prediction even without employing magnetic tuning shims; the higher order ( $n > 6$ ) multipole errors have also been small. For the KEK-built quadrupoles, the main focus has been on a re-design of the cross section to reduce the systematic  $b_{10}$  in the body. This paper summarizes the studies that used the latest expected field errors before this workshop.

## 2 EXPECTED FIELD ERRORS

The leading sources of dynamic aperture reductions are the field errors of the FNAL and KEK triplet quadrupoles. The expected errors of the FNAL quadrupoles (version 2.0) are given in Tab. 2. With the experience of model construction and measurements, and design iterations that occurred through close interaction between the magnet and accelerator physics groups, knowledge and confidence in the expected body and end-field errors has substantially improved. The KEK quadrupole errors used in the simulations reported in this article are shown in Tab. 3. However, the coil cross-section of the KEK quadrupole has been recently redesigned in order to substantially reduce the geometric  $b_{10}$  error. The new KEK error table (version 3.0) is shown in Tab. 4. These errors have not been used for simulations reported here and only serve for reference purposes.

The errors for the IPN-Novosibirsk built warm D1 are shown in Tab. 5. These errors are expected to be satis-

\* Work performed under the auspices of the US Department of Energy.

Table 2: Expected field errors of FNAL low- $\beta$  quadrupole at collision (version 2.0,  $R_{ref} = 17$  mm).  $\langle \cdot \rangle$ ,  $d(\cdot)$  and  $\sigma(\cdot)$  denote the mean, mean uncertainty and rms of the harmonics, respectively.

| $n$  | Normal                |                 |               | Skew                  |          |               |
|------|-----------------------|-----------------|---------------|-----------------------|----------|---------------|
|      | $\langle b_n \rangle$ | $d(b_n)$        | $\sigma(b_n)$ | $\langle a_n \rangle$ | $d(a_n)$ | $\sigma(a_n)$ |
| body | [unit]                |                 |               |                       |          |               |
| 3    | –                     | 0.3             | 0.8           | –                     | 0.3      | 0.8           |
| 4    | –                     | 0.2             | 0.8           | –                     | 0.2      | 0.8           |
| 5    | –                     | 0.2             | 0.3           | –                     | 0.2      | 0.3           |
| 6    | –                     | 0.6             | 0.6           | –                     | 0.05     | 0.1           |
| 7    | –                     | 0.05            | 0.06          | –                     | 0.04     | 0.06          |
| 8    | –                     | 0.03            | 0.05          | –                     | 0.03     | 0.04          |
| 9    | –                     | 0.02            | 0.03          | –                     | 0.02     | 0.02          |
| 10   | –                     | 0.02            | 0.03          | –                     | 0.02     | 0.03          |
| LE   | [unit-m]              | (length=0.41 m) |               |                       |          |               |
| 2    | –                     | –               | –             | 16.4                  | –        | –             |
| 6    | 0.82                  | 0.82            | 0.31          | –                     | 0.21     | 0.06          |
| 10   | -0.08                 | 0.08            | 0.04          | –                     | 0.04     | 0.04          |
| RE   | [unit-m]              | (length=0.33 m) |               |                       |          |               |
| 6    | –                     | 0.41            | 0.31          | –                     | –        | –             |
| 10   | -0.08                 | 0.08            | 0.04          | –                     | –        | –             |

Table 3: Expected field errors of KEK low- $\beta$  quadrupole at collision (version 2.0,  $R_{ref} = 17$  mm).

| $n$  | Normal                |                 |               | Skew                  |          |               |
|------|-----------------------|-----------------|---------------|-----------------------|----------|---------------|
|      | $\langle b_n \rangle$ | $d(b_n)$        | $\sigma(b_n)$ | $\langle a_n \rangle$ | $d(a_n)$ | $\sigma(a_n)$ |
| body | [unit]                |                 |               |                       |          |               |
| 3    | –                     | 0.51            | 1.0           | –                     | 0.51     | 1.0           |
| 4    | –                     | 0.29            | 0.57          | –                     | 0.29     | 0.57          |
| 5    | –                     | 0.19            | 0.38          | –                     | 0.19     | 0.38          |
| 6    | –                     | 0.5             | 0.19          | –                     | 0.10     | 0.19          |
| 7    | –                     | 0.05            | 0.06          | –                     | 0.05     | 0.06          |
| 8    | –                     | 0.02            | 0.03          | –                     | 0.02     | 0.03          |
| 9    | –                     | 0.01            | 0.01          | –                     | 0.01     | 0.01          |
| 10   | 0.25                  | 0.03            | 0.01          | –                     | 0.01     | 0.01          |
| LE   | [unit-m]              | (length=0.45 m) |               |                       |          |               |
| 2    | –                     | –               | –             | 13.4                  | –        | –             |
| 6    | 2.28                  | –               | –             | 0.07                  | –        | –             |
| 10   | -0.17                 | –               | –             | -0.02                 | –        | –             |

factory. The BNL built cold D1 magnets have the same coil design as the RHIC arc dipoles and their field quality is well established. These errors are shown in Tab. 6. In the next section we evaluate the dynamic aperture under nominal collision conditions and explore the optimum quadrupole arrangement to minimize the error impact.

### 3 DYNAMIC APERTURE TRACKING ANALYSIS

The leading errors of the IR quadrupoles are the systematic  $b_6$  and  $b_{10}$ , which are allowed by the quadrupole symmetry. We assess the effect of magnetic errors by the tune spread of particles with amplitudes of up to 6 times the transverse

Table 4: Expected field errors of KEK low- $\beta$  quadrupole at collision (version 3.0,  $R_{ref} = 17$  mm).

| $n$  | Normal                |                 |               | Skew                  |          |               |
|------|-----------------------|-----------------|---------------|-----------------------|----------|---------------|
|      | $\langle b_n \rangle$ | $d(b_n)$        | $\sigma(b_n)$ | $\langle a_n \rangle$ | $d(a_n)$ | $\sigma(a_n)$ |
| body | [unit]                |                 |               |                       |          |               |
| 3    | –                     | 0.50            | 1.00          | –                     | 0.50     | 1.00          |
| 4    | –                     | 0.70            | 0.80          | –                     | 0.30     | 0.80          |
| 5    | –                     | 0.20            | 0.40          | –                     | 0.20     | 0.40          |
| 6    | 0.1                   | 0.50            | 0.60          | –                     | 0.10     | 0.20          |
| 7    | –                     | 0.05            | 0.06          | –                     | 0.04     | 0.06          |
| 8    | –                     | 0.03            | 0.05          | –                     | 0.02     | 0.04          |
| 9    | –                     | 0.02            | 0.03          | –                     | 0.02     | 0.02          |
| 10   | –                     | 0.10            | 0.05          | –                     | 0.02     | 0.03          |
| LE   | [unit-m]              | (length=0.45 m) |               |                       |          |               |
| 2    | –                     | –               | –             | 13.4                  | –        | –             |
| 6    | 2.28                  | –               | –             | 0.07                  | –        | –             |
| 10   | -0.17                 | –               | –             | -0.02                 | –        | –             |

Table 5: Expected field errors of Novosibirsk-built warm dipoles (D1) at collision (version 1.0,  $R_{ref} = 17$  mm).

| $n$  | Normal                |          |               | Skew                  |          |               |
|------|-----------------------|----------|---------------|-----------------------|----------|---------------|
|      | $\langle b_n \rangle$ | $d(b_n)$ | $\sigma(b_n)$ | $\langle a_n \rangle$ | $d(a_n)$ | $\sigma(a_n)$ |
| body | [unit]                |          |               |                       |          |               |
| 3    | 0.3                   | 0.1      | 0.06          | –                     | –        | –             |
| 5    | 0.1                   | 0.05     | 0.03          | –                     | –        | –             |
| 7    | -0.02                 | 0.005    | 0.003         | –                     | –        | –             |
| 9    | -0.02                 | 0.005    | 0.003         | –                     | –        | –             |
| 11   | -0.04                 | 0.005    | 0.003         | –                     | –        | –             |
| 13   | 0.04                  | 0.005    | 0.003         | –                     | –        | –             |

rms beam size ( $6\sigma_{xy}$ ), and by the dynamic aperture determined by 6D TEAPOT [5] tracking after either  $10^3$  or  $10^5$  turns, averaged over 10 random sets of magnetic errors at 5 emittance ratios  $\epsilon_x/\epsilon_y$ . Tracked particles have 2.5 times the rms momentum deviation ( $2.5\sigma_p$ ) [3, 4]. Uncertainties in the mean are set at their full amount with either plus or minus sign. Due to computing power limitations, we track particles in most cases for only 1,000 turns. In Sec. 3.2 we show the difference in the dynamic aperture when particles are tracked up to 100,000 turns.

#### 3.1 Tracking results

The tune spread due to multipole errors scales as  $(x_c + \sqrt{\beta_{xy}\epsilon_{xy}})^{n/2}/\epsilon_{xy}^{n/2}$ , where  $x_c$  is the closed orbit,  $\beta_{xy}$  the lattice  $\beta$ -function and  $\epsilon_{xy}$  the emittance. The  $b_{10}$  error of the KEK magnets alone produces a tune spread of  $0.61 \times 10^{-3}$  at  $6\sigma_{xy}$  thereby reducing the dynamic aperture by  $2\sigma_{xy}$  (Tab. 7).

A possibility for reducing the impact of the KEK geometric  $b_{10}$  could be to adopt a “mixed” triplet scheme where Q1 and Q3 are KEK quadrupoles and Q2 FNAL quadrupoles. This arrangement would lead to a 30% reduction of the tune spread, and an 18% increase of the dynamic

Table 6: Expected field errors of BNL-built cold dipoles (D1) at collision (version 1.0,  $R_{ref} = 25$  mm).

| $n$  | Normal                |          |               | Skew                  |          |               |
|------|-----------------------|----------|---------------|-----------------------|----------|---------------|
|      | $\langle b_n \rangle$ | $d(b_n)$ | $\sigma(b_n)$ | $\langle a_n \rangle$ | $d(a_n)$ | $\sigma(a_n)$ |
| body | [unit]                |          |               |                       |          |               |
| 2    | 0.10                  | 0.80     | 0.28          | 0.63                  | 3.47     | 1.55          |
| 3    | -3.30                 | 3.43     | 1.82          | -0.26                 | 0.58     | 0.21          |
| 4    | 0.01                  | 0.25     | 0.09          | 0.04                  | 1.08     | 0.42          |
| 5    | 0.53                  | 0.81     | 0.41          | -0.07                 | 0.19     | 0.06          |
| 6    | -0.14                 | 0.12     | 0.04          | -0.05                 | 0.56     | 0.17          |
| 7    | 1.14                  | 0.20     | 0.11          | -0.01                 | 0.07     | 0.03          |
| 8    | -0.01                 | 0.04     | 0.01          | -0.01                 | 0.15     | 0.05          |
| 9    | 0.01                  | 0.12     | 0.05          | -0.01                 | 0.03     | 0.01          |
| 10   | 0.05                  | 0.06     | 0.02          | 0.04                  | 0.04     | 0.02          |
| 11   | -0.57                 | 0.04     | 0.02          | -0.01                 | 0.02     | 0.01          |
| LE   | [unit-m]              |          |               |                       |          |               |
| 2    | -0.47                 | 2.26     | 0.99          | -1.42                 | 4.27     | 1.77          |
| 3    | 22.35                 | 2.93     | 1.10          | -9.85                 | 1.01     | 0.39          |
| 4    | 0.04                  | 0.73     | 0.23          | 0.09                  | 0.75     | 0.29          |
| 5    | -0.43                 | 0.69     | 0.22          | 2.23                  | 0.30     | 0.13          |
| 6    | 0.02                  | 0.29     | 0.12          | 0.01                  | 0.29     | 0.10          |
| 7    | 0.92                  | 0.11     | 0.05          | -0.86                 | 0.13     | 0.06          |
| 8    | –                     | 0.06     | 0.03          | -0.02                 | 0.08     | 0.03          |
| 9    | -0.04                 | 0.08     | 0.03          | 0.25                  | 0.05     | 0.02          |
| 10   | -0.01                 | 0.08     | 0.03          | -0.01                 | 0.04     | 0.02          |
| 11   | -0.06                 | 0.03     | 0.01          | -0.04                 | 0.02     | 0.01          |
| RE   | [unit-m]              |          |               |                       |          |               |
| 2    | 0.22                  | 1.81     | 0.66          | 0.91                  | 4.50     | 1.91          |
| 3    | 6.08                  | 2.67     | 1.16          | 0.29                  | 1.03     | 0.34          |
| 4    | –                     | 0.36     | 0.16          | 0.24                  | 0.73     | 0.31          |
| 5    | 0.03                  | 0.66     | 0.23          | –                     | 0.31     | 0.11          |
| 6    | 0.03                  | 0.17     | 0.06          | -0.01                 | 0.24     | 0.10          |
| 7    | -0.04                 | 0.13     | 0.06          | -0.03                 | 0.12     | 0.05          |
| 8    | -0.03                 | 0.07     | 0.03          | -0.02                 | 0.11     | 0.04          |
| 9    | -0.17                 | 0.08     | 0.03          | –                     | 0.05     | 0.02          |
| 10   | -0.07                 | 0.08     | 0.04          | -0.02                 | 0.10     | 0.05          |
| 11   | -0.12                 | 0.04     | 0.01          | 0.01                  | 0.02     | 0.01          |

aperture, as shown in Tab. 7.

The mixed arrangement increases the possibility for magnet sorting [6, 7] and helps randomizing the uncertainty. It may also reduce the number of needed spare magnets and simplifies the engineering process. However, combining quadrupoles of different transfer functions implies a more complicated powering scheme. While a common bus is still possible, issues that need to be investigated are the natural compensation of ripple in a triplet and the dynamic behavior at injection related to snap back and eddy-current effects [8].

In order to estimate the  $b_6$  impact, we assume that FNAL magnets are placed at IP1 and 5 and gradually decrease the total  $b_6$  to 30% of its original value assuming a positive  $d(b_6)$ . Tab. 7 shows a steady increase of the dynamic aperture from  $9.3\sigma_{xy}$  to  $12.1\sigma_{xy}$ .

The orientation of the quadrupoles was chosen to min-

Table 7: Comparison of dynamic aperture (DA) for various triplet arrangements ( $10^3$ -turn DA in units of  $\sigma_{xy}$  with  $1\sigma_{xy}$  step size).

| Case                               | DA mean | DA rms | DA min |
|------------------------------------|---------|--------|--------|
| FNAL IP5, 8; KEK IP1, 2:           |         |        |        |
|                                    | 8.5     | 1.4    | 7      |
| without $b_{10}$                   | 10.3    | 1.5    | 7      |
| FNAL as Q2; KEK as Q1, Q3 (mixed): |         |        |        |
|                                    | 10.0    | 1.5    | 8      |
| reversed Q3 LE                     | 9.6     | 2.0    | 6      |
| FNAL IP1, 5; KEK IP2, 8:           |         |        |        |
|                                    | 9.3     | 2.1    | 6      |
| 80% $b_6$                          | 9.9     | 2.0    | 6      |
| 50% $b_6$                          | 11.0    | 1.8    | 8      |
| 30% $b_6$                          | 12.1    | 1.7    | 9      |

imize the lead end  $b_6$  impact [3, 4]. With the mixed quadrupole scheme, the minimization is less effective however. In order to reduce the number of electric buses through Q3, it was further suggested to reverse the orientation of Q3. This leads to a reduction of the average dynamic aperture of  $0.4\sigma$ , and to an increase of the  $b_6$  corrector strength. As the random  $b_6$  is large, this effect could be alleviated by sorting [6, 7].

### 3.2 Short versus long term tracking

We re-confirmed [3] the difference between the dynamic aperture determined after  $10^3$  and  $10^5$  turns for two selected cases, an uncorrected machine with a small dynamic aperture and a machine that has a large dynamic aperture due to a costly correction scheme, named “scheme 4” in Ref. [9]. The difference (Tab. 8) is  $0.7\sigma_{xy}$  or 7% for the uncorrected case, and  $0.9\sigma_{xy}$  or 5% for the corrected case.

Table 8: Comparison of 1,000-turn and 100,000-turn dynamic aperture (DA).

| Case                     | DA mean | DA rms | DA min |
|--------------------------|---------|--------|--------|
| no correction ( $10^3$ ) | 10.0    | 1.5    | 8      |
| no correction ( $10^5$ ) | 9.3     | 1.4    | 7      |
| scheme 4 ( $10^3$ )      | 17.6    | 1.6    | 14     |
| scheme 4 ( $10^5$ )      | 16.7    | 1.5    | 13     |
| target ( $10^5$ )        | 12      | –      | 10     |

## 4 SUMMARY

With the error tables used in this study we find that the systematic  $b_{10}$  error is the leading source of a dynamic aperture reduction followed by the random  $b_6$  error. Mixing magnets of different origin can help reach the target dynamic aperture as it gives an improvement of about  $1.5\sigma_{xy}$ . This would be equivalent to a reduction of the systematic

$b_{10}$  and uncertainty of  $b_6$  errors by about 50%. Further benefits of mixing could be expected through the randomization of the uncertainties and a broader selection of magnets. We expect that the new KEK error table (version 3.0) with an eliminated systematic  $b_{10}$  gives a substantially better dynamic aperture.

We thank J. Gareyte, J.-P. Koutchouk, O. Brüning and J. Miles for lattice assistance and discussions, and many others, including M. Harrison, A. Ijspeert, J. Kerby, M.J. Lamm, S. Peggs, T. Sen, R. Talman, T. Taylor and A.V. Zlobin.

## 5 REFERENCES

- [1] V. Ptitsin, W. Fischer, J. Wei, “LHC interaction region region correction in heavy ion operation”, these proceedings.
- [2] J. Wei, “Principle of interaction region local correction”, these proceedings.
- [3] J. Wei et al., “US-LHC IR magnet error analysis and compensation”, EPAC 1998 proceedings (1998) p. 380.
- [4] J. Wei et al., “Interaction region local correction for the Large Hadron Collider”, PAC 1999 proceedings (1999) p. 2921.
- [5] L. Schachinger, R. Talman, Part. Accel. **22**, 35 (1987).
- [6] J. Wei, R. Gupta, M. Harrison, A. Jain, et al, PAC99 (1999).
- [7] J. Shi, Nuclear Instruments and Methods A (1999).
- [8] J-P. Koutchouk, private communications.
- [9] W. Fischer et al., “LHC interaction region correction scheme studies”, these proceedings.